INVERSE PROBLEMS

SHIRO KUBO (Editor)

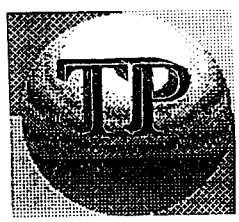

ATLANTA TECHNOLOGY PUBLICATIONS
P.O. Box 77032
Atlanta, Georgia 30357, USA

Inverse Design of Three-Dimensional Shapes with Overspecified Thermal Boundary Conditions

George S. Dulikravich
Department of Aerospace Engineering
The Pennsylvania State University
University Park, PA 16802, USA

Thomas J. Martin
Department of Aerospace Engineering
The Pennsylvania State University
University Park, PA 16802, USA

Abstract

This paper is concerned with the inverse design of coolant flow passages in three-dimensional solid objects by overspecifying thermal boundary conditions. The optimization algorithm used in this inverse design code is based on a quasi-Newton gradient search method. A simple method for escaping local minima has been implemented and involves switching the objective function when a stationary point is achieved. The analysis of three-dimensional, non-linear heat conduction problems was done with a boundary element formulation because of its speed and accuracy. The user is free to supply either temperature or heat flux boundary conditions or both. Optimization methods implemented minimize the difference between any over specified boundary conditions and values computed by the boundary element algorithm.

Introduction

The mathematical model for steady state, nonlinear heat conduction can be represented by a boundary value problem over a multiply-connected domain. Boundary conditions of Dirichlet or Neumann type are specified on both the inner (hole or coolant passage) surfaces and the outer boundary. If the problem is well-posed, the solution for a particular geometry is unique. If the boundary conditions are over specified, then the problem may be solved by altering the configuration of the holes. Such is the case for the inverse shape design methodology presented herein. Earlier applications of inverse shape design and optimization were done for turbine blade coolant flow passages in two dimensions by Kennon and Dulikravich (1985, 1986a, 1986b). They used error between the specified heat fluxes on the outer (hot) surface and the computed heat fluxes obtained there by analyzing the temperature field (Brebbia and Dominguez, 1989) for the current configuration of cooling holes. This objective function was then minimized using the Fletcher-Reeves gradient search method (Vanderplaats, 1984). Since then, this inverse design procedure has been enhanced to include blades with ceramic coating (Chiang and Dulikravich, 1986), satisfaction of manufacturing constraints via a penalty function (Chiang and Dulikravich, 1986; Dulikravich, 1988) and ability to handle mixed boundary conditions and cross-sectional shapes belonging to a family of inclined Lame curves (Dulikravich, 1992; Dulikravich and Martin,

1992a, 1992b, 1992c). The same methodology has been extended in this paper into fully three-dimensional inverse design with temperature-dependent material properties for the first time.

The Optimization Technique

The complexity of the analysis of the temperature field in an irregular, three-dimensional, multiply-connected domain calls for the use of a relatively simple but robust and fast optimization technique for constrained nonlinear optimization. The Davidon-Fletcher-Powell (DFP) (Vanderplaats, 1984; Arora, 1989) quasi-Newton algorithm was implemented because it requires a relatively low number of objective function evaluations and of its ability to converge quickly near minima. A first-order numerical approximation was used to compute gradients of the objective function. Line search was handled using quadratic polynomial fitting. Several different optimization procedures were tested such as a quadratic programming method and spline fitting interpolation (Dulikravich, 1988; Dulikravich and Martin, 1992c) to find the minimum in the search direction. Each procedure had certain advantages in particular instances while the DFP algorithm proved to be the most reliable. For example, the quadratic programming method (Pshenichny and Danilin, 1969) reduced the cost function relatively quickly when the current geometry was far from the converged geometry, but performed poorly when near the converged solution.

The geometry of the internal holes make up the design variables of the objective function. Since the number of holes may also be a design variable, a problem arises when computing the gradient of the objective function. Additional holes cannot easily be added since the gradient search direction should include all the possible combinations of hole location and geometry. A simple and straightforward approach is to start optimizing with a large number of holes (limited by computer memory and computational efficiency) and then reduce the number of holes during the optimization procedure. The criterion for excluding a particular hole is when the hole reduces to such a small size that it has a negligible effect on the heat flux at the outer boundary (Dulikravich and Kosovic, 1992). Otherwise, the procedure is time consuming and often terminates in a local minima.

During the optimization process local minimas can occur and halt the process before achieving an optimal solution. In order to overcome such a situation, a simple technique has been devised (Dulikravich, 1988). In this approach, whenever the optimization stalls, the formulation of the objective function is automatically switched. The new objective function provides a departure from the local minima and further convergence towards the global minimum. Specifically, the objective is to minimize the difference between the specified values, U^{spec}, and the calculated values, U^{calc},

which can be either temperature or heat flux at the outer boundary. The objective function F can be mathematically formulated as an L2 norm of the global error

$$f(\mathbf{x}) = \frac{\sum_{j=1}^{N} (U_j^{spec} - U_j^{calc})^2}{\sum_{j=1}^{N} (U_j^{spec})^2 + \varepsilon} \tag{1}$$

or as a local normalized error at each panel on the outer boundary.

$$f(\mathbf{x}) = \sum_{j=1}^{N} \frac{(U^{spec} - U^{calc})^2_j}{(U^{spec})^2_j + \varepsilon} \tag{2}$$

Here, ε is a very small user-specified parameter to avoid division by zero. In summary, the optimization procedure consists of the following steps.

(1) Specify the shape of the outer surface and coating (if any) of the object.

(2) Specify the required boundary conditions on the outer and inner coolant passage surfaces needed to solve the boundary value problem.

(3) Specify the additional boundary conditions on the outer surface (either temperature or heat flux depending upon which is being computed by the BEM) or temperatures at internal nodes in the domain.

(4) Specify manufacturing constraints such as the minimum distance between holes and the outer or interface metal/coating surface.

(5) Specify an initial guess for the internal cooling hole geometries. These are the design variables of the cost function and can take a variety of forms (Kennon and Dulikravich ,1985, 1986a, 1986b; Dulikravich and Martin, 1992a, 1992b, 1992c)

(6) Using the BEM, unknowns at the outer boundaries are computed and the composite objective function is formed. The gradient of this function must be computed at each optimization cycle and requires one BEM analysis call per each design variable to find a descent direction.

(7) In the direction of the gradient, different values of the line search parameter α, which determines the distance in the search direction, are found and an optimum determined by a quadratic polynomial or exponential spline fitting and interpolation (Dulikravich, 1988).

(8) The design variables are updated at the computed optimal value along the line search direction. The DFP technique is used to update the search direction for the next optimization cycle.

(9) If the optimization procedure stalls in a local minimum, the objective function is automatically switched and the optimization is continued from step (6).

Boundary Element Formulation

Many engineering problems such as heat conduction, incompressible fluid flow and electric field problems are governed by the Laplace's equation

$$\nabla^2 u' = 0 \tag{3}$$

with boundary conditions prescribed on surface Γ bounding the arbitrarily shaped three-dimensional domain. By introducing an approximation, u(x,y,z), an error is introduced, called the residual, and is normally non-zero unless u is the exact solution. The weighted average of the residual may be set to zero by the weighted residual statement

$$\int_{\Omega} u^* \nabla^2 u \, d\Omega = 0 \tag{4}$$

where u* represents the weight function and is sometimes called the fundamental solution. Integrating by parts twice, we obtain the boundary element equation (which is a form of Green's theorem)

$$\int_{\Omega} u \nabla^2 u^* \, d\Omega + \int_{\Gamma} u^* q \, d\Gamma = \int_{\Gamma} q^* u \, d\Gamma \tag{5}$$

where $q = \partial u/\partial n$ and $q^* = \partial u^*/\partial n$ and n is the direction of the outward normal to the surface Γ. The fundamental solution is forced to satisfy the auxiliary equation of Laplace's equation and the homogeneous boundary conditions and thus is a Green's function solution corresponding to an applied unit potential concentrated at a point $\mathbf{x}(\xi,\eta,\zeta)$

$$u^* = \frac{1}{4\pi r} \tag{6}$$

where $r = |\mathbf{x} - \mathbf{X}|$. The bounding surface is discretized into M surface elements and N3 nodes at which potentials, u, and potential derivatives, q, are linearly distributed. The boundary element equation in discretized form becomes

$$c_i u_i + \sum_{j=1}^{Nsp} \int_{\Gamma_j} u \, q^* \, d\Gamma_j = \sum_{j=1}^{Nsp} \int_{\Gamma_j} q \, u^* \, d\Gamma_j \tag{7}$$

for each ith node. The term c_i indicates the scaled internal angle due to having only a portion of the domain contained at the ith surface node. The whole set of equations for the N nodes can be expressed in matrix form

$$[\mathbf{H}]\,\mathbf{U} = [\mathbf{G}]\,\mathbf{Q} \tag{8}$$

The c_i coefficients make up the diagonal of the H matrix and may be computed explicitly by calculation of the internal angle at the node or implicitly (Brebbia, 1989) by assuming a constant potential throughout the entire domain

$$\mathbf{H}_{ii} = - \sum_{j=1}^{N_N} \mathbf{H}_{ij} \qquad i \neq j \tag{9}$$

Equation (9) is better suited for numerical implementation due to round-off errors that occur in the matrix formulation and solution. Computing the diagonal implicitly tends to distribute the error throughout the domain rather than having it contained on the main diagonal.

Potential boundary conditions are specified at N1 nodes and potential derivatives at N2 nodes such that at least one value is known at each node and N1 + N2 = N3. The equations can then be reordered into a system of linear algebraic equations of the form

$$[\mathbf{A}]\,\mathbf{X} = \mathbf{F} \tag{10}$$

Nonlinear, Steady-State Heat Conduction Formulation

The governing equation for steady-state heat conduction in a solid with temperature dependent material properties is expressed as

$$\nabla \cdot (\lambda(T)\, \nabla T) = 0 \tag{11}$$

where T is the temperature and $\lambda(T)$ is the temperature-dependent thermal conductivity. The heat function, u, is defined by using the classical Kirchoff transformation as follows

$$u = \int_0^T \frac{\lambda(T)}{\lambda o}\, dT \tag{12}$$

where $\lambda(T)$ is given as a function of the form

$$\lambda(T) = \lambda o\, (A / T + B + C\, T + D\, T^2 + E\, T^3) \tag{13}$$

Using (12), we obtain Laplace's equation for the heat function or potential u (see Equation 3). The boundary conditions are also easily transformed using (12). Equation (3) can then be directly solved by the boundary element method for the heat function u and temperatures and heat fluxes recovered using the inverse Kirchoff transformation.

Verification of the Nonlinear Boundary Element Formulation

A computer program has been developed that is based on the theory discussed in the previous sections and computational results were obtained for a few sample problems. The accuracy of the boundary element analysis program for nonlinear heat conduction in a parallelepiped object was verified. Four sides of the object were kept adiabatic (q = 0) and the other two opposite planes were subject to different temperatures (T = 100 ^{o}C and T = 0 ^{o}C). The reference thermal conductivity and other parameters of equation (13) were specified (λo = 1.0 kcal/ms^{o}C, B = 1.0, A = D = E = 0) and temperature data was collected for various degrees of non linearity given by one parameter C. The results (Fig. 1) were found to compare well with the analytic solution and results obtained with the NASTRAN finite element program (Tanaka, Kikuta and Togoh, 1987).

Inverse Design of a Three-Dimensional Super-Elliptic Cavity Within a Sphere

This test case was used to demonstrate the fully three-dimensional inverse design capability of the optimization algorithm with the BEM code. The geometry consisted of a unit sphere with an off-centered cavity of a three-dimensional super-elliptic shape given by

$$\left(\frac{x' - x_0}{a}\right)^N + \left(\frac{y' - y_0}{b}\right)^N + \left(\frac{z' - z_0}{c}\right)^N = 1 \qquad (14)$$

Seven design variables are derived from this equation: the center of the super-elliptic cavity (xo,yo,zo), its semi-major axes (a,b,c) and the super-elliptic exponent, N (Table 1).

xo	yo	zo	a	b	c	N
0.2	0.2	0.2	0.3	0.4	0.5	4.0

Table 1. Initial Design Variables for a 3-D Off-Centered Super-Elliptic Cavity Within a Sphere.

The outer spherical surface and the internal super-elliptical cavity (Fig. 2) were discretized with the same number (64) of isoparametric quadrilateral flat panels. A temperature of 100 ^{o}C was specified on the outer surface and 50 ^{o}C on the inner super-elliptic surface. The material properties were assumed such that the thermal conductivity λo = 0.00534 kcal/m s ^{o}C, A = D = E = 0, B = 1.0, and C = -0.000055066 1/^{o}C. The temperature derivative specified on the outer surface was taken from the analytic solution ($\partial T/\partial n$ = 59.3 ^{o}C/m) corresponding to the desired (target) configuration consisting of a centered spherical cavity (radius 0.5 m). Figure 3 depicts the convergence history of the composite objective function. Note that a spike occurs at the 30th

iteration indicating an automatic cost function switch from global to local L2 norm. The run was terminated near the global minimum with an objective function value of 0.32%. The DFP optimization algorithm nearly reached the fully converged sphere-within-a-sphere configuration (Fig. 4) in 50 optimization cycles. The entire optimization procedure required 647 calls to the BEM analysis routine and consumed approximately 2235 seconds of CPU time on an IBM 3090.

Inverse Design of a Finned Coolant Flow Passage in the Wall of a Cylindrical Duct

This test case was developed to demonstrate the capability of the inverse design algorithm in handling a different set of design variables. The duct wall was described as a cylindrical shell with N = 72 identically shaped and sized coolant passages positioned equidistantly in the annular region and running in the axial direction (Fig. 5). The duct outer and inner radii of 1.0 m and 0.5 m, respectively, were specified at three axial locations. The inner duct surface will be called the hot surface and the outer duct surface the shroud. The coolant passage was defined in a similar fashion by specifying its outer and inner radii (R_o and R_i respectively) and the width of the passage. In addition, the inner surface of the coolant passage was fitted with a fin described by

$$R_{fin} = R_i + A \sin^m (P\theta) \tag{15}$$

where R_i is the inner radius of the coolant passage and A is the height of the fin at the centerline. For this test case, the five design variables are R_o, R_i, A, m and P, where P is the percentage of the angle $\theta = 2\,\Pi / N$ that indicates the coolant passage width. The symmetry of the object about the meridional plane through center of the passage was utilized such that only the right-hand-side half of one passage and the bounding solid were modeled. The initial guess design variables and the target design variables are given in Table 2 and Table 3.

Ri	Ro	P	A	m
0.80	0.65	0.40	0.05	2.0

Table 2. Initial Design Variables for the Finned Coolant Flow Passage in a Cylindrical Duct Wall.

Ri	Ro	P	A	m
0.90	0.60	0.50	0.20	6.0

Table 3 Target Design Variables for the Finned Coolant Flow Passage in a Cylindrical Duct Wall.

A total of 106 flat panels modeled the entire geometry with 2800 K specified on the hot surface and 300 K on the shroud. The periodic meridional surfaces between the passages are adiabatic (q = 0).

Temperatures specified on the coolant passage walls varied radially between 600 K at R_i and 100 K at R_o and the thermal conductivity was the same as in the case of a sphere. The BEM algorithm was run once with a particular (converged) geometry to generate the heat flux boundary conditions on the outer surface to be used in the optimization. The DFP algorithm reduced the cost function to 0.46% in 74 iterations (Fig. 6) with a total of four automatic switches in the cost function. Figure 7 shows a cross section of the three-dimensional coolant passage. The bold lines show the outer surface and the fully converged geometry of the coolant passage and the fin. The dotted lines depict the initial guess geometry and the thin solid lines are intermediate geometries. The final geometry differed from the converged geometry only in the exponent design variable (final m = 5.6 instead of m = 6.0). The entire optimization procedure required 957 calls to the BEM analysis routine and about 2600 seconds of CPU time on an IBM 3090.

Inverse Design of a 3-D Finned Coolant Flow Passage in a Parabolic Rocket Nozzle Wall

We used a realistically shaped rocket nozzle with the same geometry specifications as the previous test case except now the design variables and outer surface geometry vary at each axial location. The nozzle section was modeled at five axial locations yielding a shape optimization problem having 25 design variables. The thermal conductivity parameters and boundary conditions were specified identical to those of the cylindrical duct. The initial design variables are given in Table 4.

Ri	Ro	P	A	m
0.55	0.50	0.75	0.05	4.00
0.65	0.60	0.75	0.05	4.00
0.75	0.70	0.75	0.05	4.00
0.85	0.80	0.75	0.05	4.00
0.95	0.90	0.75	0.05	4.00

Table 4. Initial Design Variables for the Optimization of a Three-Dimensional Finned Coolant Flow Passage in a Parabolic Rocket Nozzle.

Figure 8 depicts the convergence history of the optimization process that was completed after 111 iterations and reduced the cost function to 0.56%. The initial guesses and the fully converged local finned cross sections are shown in Figure 9. The final design variables (Table 5) differed somewhat from the target geometry (Table 6). The procedure was terminated by the user prematurely near the global minimum. The procedure could have been continued on its search for the global minimum if desired although to reduce the cost function further would probably require

another 100 optimization cycles. The algorithm seemed to have difficulty reaching the converged coolant passage and fin width probably because both of these design variables have similar effects on the geometry. The entire optimization procedure required 3235 calls to the BEM analysis routine and used 12,900 seconds of CPU time on an IBM 3090 computer.

Ri	Ro	P	A	m
0.65	0.39	0.45	0.21	2.30
0.74	0.50	0.57	0.20	2.91
0.84	0.61	0.58	0.20	3.38
0.93	0.70	0.61	0.19	3.22
1.02	0.80	0.70	0.20	2.73

Table 5. Final Design Variables for the 3-D Finned Coolant Flow Passage in a Parabolic Nozzle.

Ri	Ro	P	A	m
0.65	0.40	0.50	0.20	2.00
0.75	0.50	0.50	0.20	2.00
0.85	0.60	0.50	0.20	2.00
0.95	0.70	0.50	0.20	2.00
1.05	0.80	0.50	0.20	2.00

Table 6. Target Design Variables of the 3-D Finned Coolant Flow Passage in a Parabolic Nozzle.

Summary

The concept of inverse design of three-dimensional configurations subject to over-specified thermal boundary conditions has been found to be feasible. Future research possibilities in the field of three-dimensional inverse design using the presented methodology could be directed toward complex design tools involving thermal convection, radiation and conduction as well as thermal stress-deformation field analysis and electromagnetic field problems. The same optimization procedure with boundary integral analysis described herein can be used for problems governed by Poisson's equation. This work is presently being extended into unsteady, fully three-dimensional, nonlinear heat conduction involving latent heat and multiple domains with different properties.

References

Arora, J.S., Introduction to Optimum Design, McGraw-Hill Book Company, 1989.

Brebbia, C.A. and Dominguez, J., Boundary Elements: An Introductory Course, McGraw-Hill Book Company, 1989.

Chiang, T.L. and Dulikravich, G.S., "Inverse Design of Composite Turbine Blade Circular Coolant Flow Passages", *ASME J. of Turbomachinery*, Vol. 108, pp. 275-282, 1986.

Dulikravich, G.S., "Inverse Design and Active Control Concepts in Strong Unsteady Heat Conduction", *Applied Mechanics Reviews*, Vol. 41, No. 6, June 1988, pp. 270-277, 1988.

Dulikravich, G.S., "Inverse Design of Proper Number, Shapes, Sizes and Locations of Coolant Flow Passages", *Proceedings of the 10th Annual CFD Workshop*, Editor: R. Williams, NASA MSFC, Huntsville, AL, April 28-30, 1992

Dulikravich, G.S. and Hayes, L.J., "Control of Surface Temperatures to Optimize Survival in Cryopreservation, ASME Winter Annual Meeting", *Proceedings of the Symposium on Computational Methods in Bioengineering*, Editors: R.L. Spilker and B.R. Simon, BED-Vol. 9, pp. 255-265, Nov. 27 - Dec. 2, 1988.

Dulikravich, G.S. and Kosovic, B., "Minimization of the Number of Cooling Holes in Internally Cooled Turbine Blades", *International Journal of Turbo & Jet Engines*, Vol. 9, No. 4, pp. 277-283, 1992.

Dulikravich, G.S. and Martin, T.J., "Determination of Void Shapes, Sizes and Locations Inside an Object with Known Surface Temperatures and Heat Fluxes", *Proceedings of the IUTAM Symposium on Inverse Problems in Engineering Mechanics*, Editors: M. Tanaka and H.D. Bui, Tokyo, Japan, May 11-15, 1992a.

Dulikravich, G.S. and Martin, T.J., "Determination of the Proper Number, Locations, Sizes and Shapes of Super elliptic Coolant Flow Passages in Turbine Blades", *Proceedings of the International Symposium on Heat and Mass Transfer in Turbomachinery (ICHMT)*, Editor: R.J. Goldstein, Athens, Greece, Aug. 24-28, 1992b.

Dulikravich, G.S. and Martin, T.J., "Inverse Design of Super Elliptic Coolant Passages in Coated Turbine Blades with Specified Temperatures and Heat Fluxes", Symposium on Multidisciplinary Analysis and Optimizations (AIAA/USAF/NASA/ OAI), *AIAA paper 92-4714*, Cleveland, OH, Sept. 21-23, 1992c; to appear in *AIAA J. of Thermophysics and Heat Transfer*.

Kennon, S.R., and Dulikravich, G.S., "The Inverse Design of Internally Cooled Turbine Blades", *ASME Journal of Engineering for Gas Turbines and Power*, pp. 123-126, January 1985.

Kennon, S.R. and Dulikravich, G.S., "Inverse Design of Multi-holed Internally Cooled Turbine Blades", *Internat. J. of Numerical Methods in Engineering*, Vol. 22, pp. 363-375, 1986a.

Kennon, S.R. and Dulikravich, G.S., "Inverse Design of Coolant Flow Passage Shapes with Partially Fixed Internal Geometries", *International Journal of Turbo & Jet Engines*, Vol. 3., No. 1, pp. 13-20, 1986b.

Pshenichny, B.N. and Danilin, Y.M., Numerical Methods in Extremal Problems, MIR Publishers, Moscow, 1969.

Tanaka, M., Kikuta, M., and Togoh, H., "Boundary Element Analysis of Nonlinear Transient Heat Conduction Problems", *Computer Methods in Applied Mechanics and Engineering*, Vol. 62, No. 3, pp. 321-329, June 1987.

Vanderplaats, G.N., Numerical Optimization Techniques for Engineering Design, McGraw-Hill, New York, 1984.

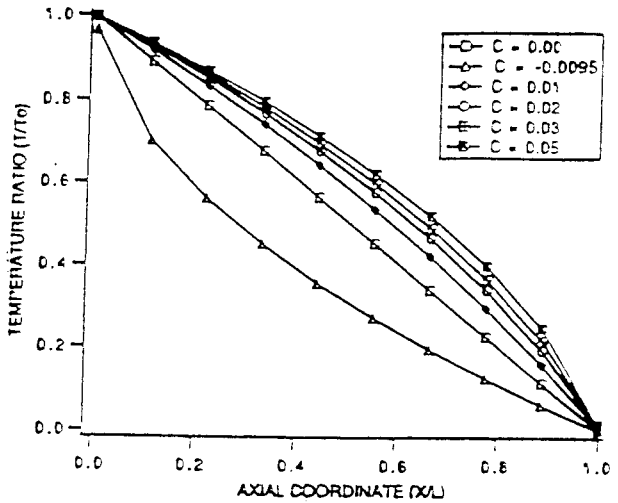

Figure 1. Temperature distribution for various degrees of thermal diffusivity non-linearity.

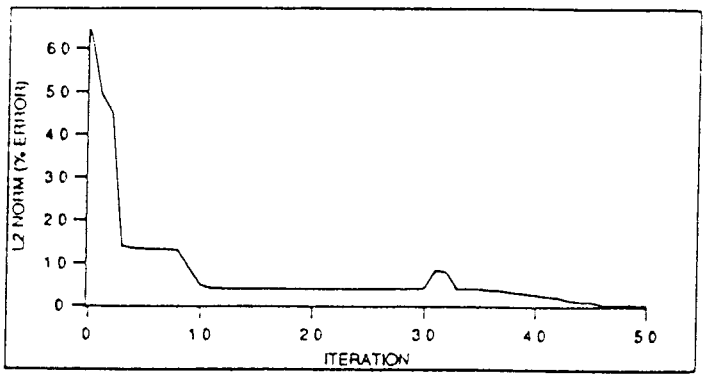

Figure 2. Convergence history of the inverse design of a super-elliptic cavity within a sphere.

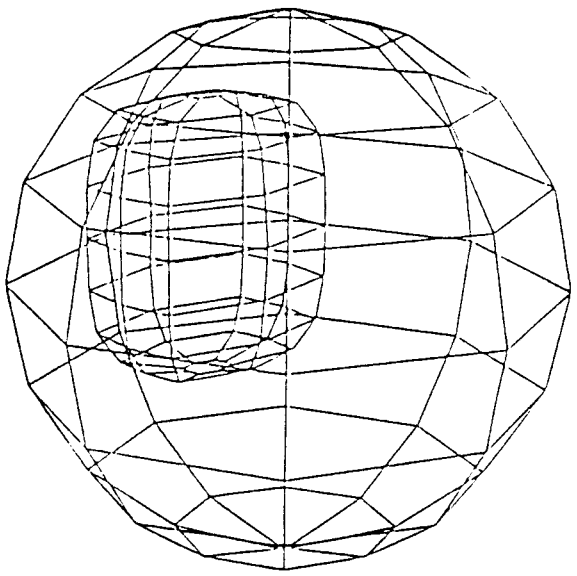

Figure 3. Initial guess geometry of a super-elliptic off-center cavity within a sphere.

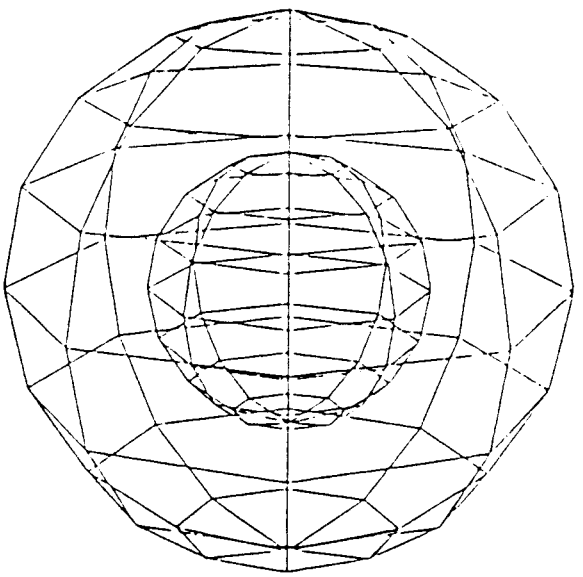

Figure 4. Fully converged geometry of a super-elliptic cavity within a sphere.

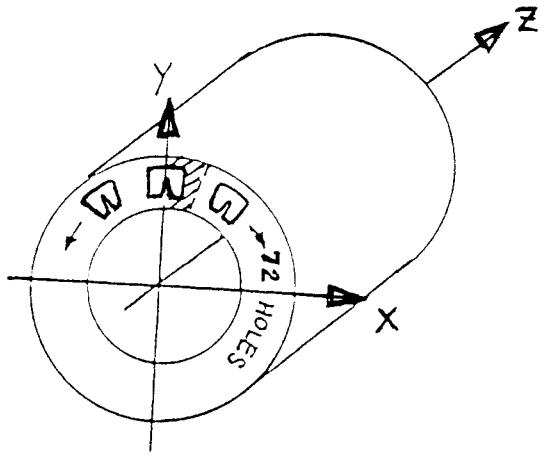

Figure 5. A sketch of the entire duct shape with an indication of coolant flow passages.

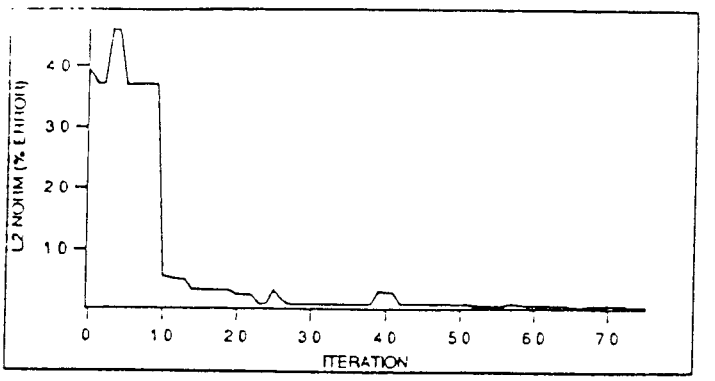

Figure 6. Convergence history of the inverse design of a finned coolant flow passage in a cylindrical duct.

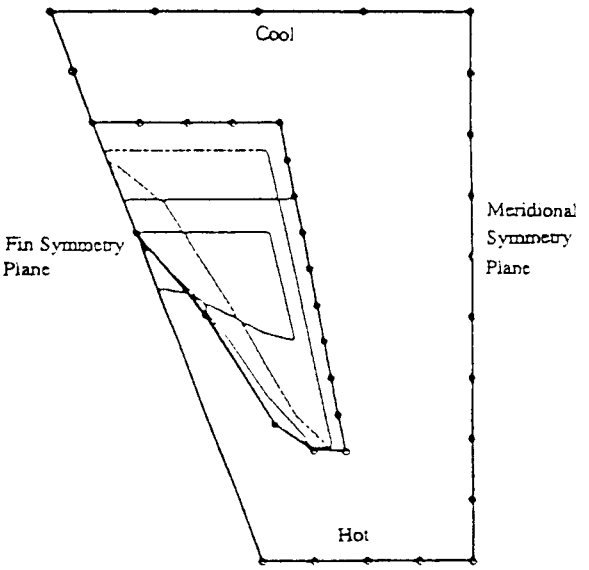

Figure 7. Cross-sectional geometry variation during the optimization process for a finned coolant flow passage in a cylindrical duct.

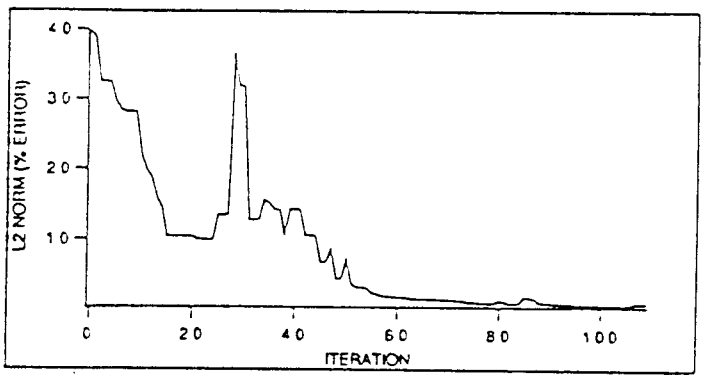

Figure 8. Convergence history for the inverse design of a 3-D finned coolant flow passage in a parabolic nozzle.

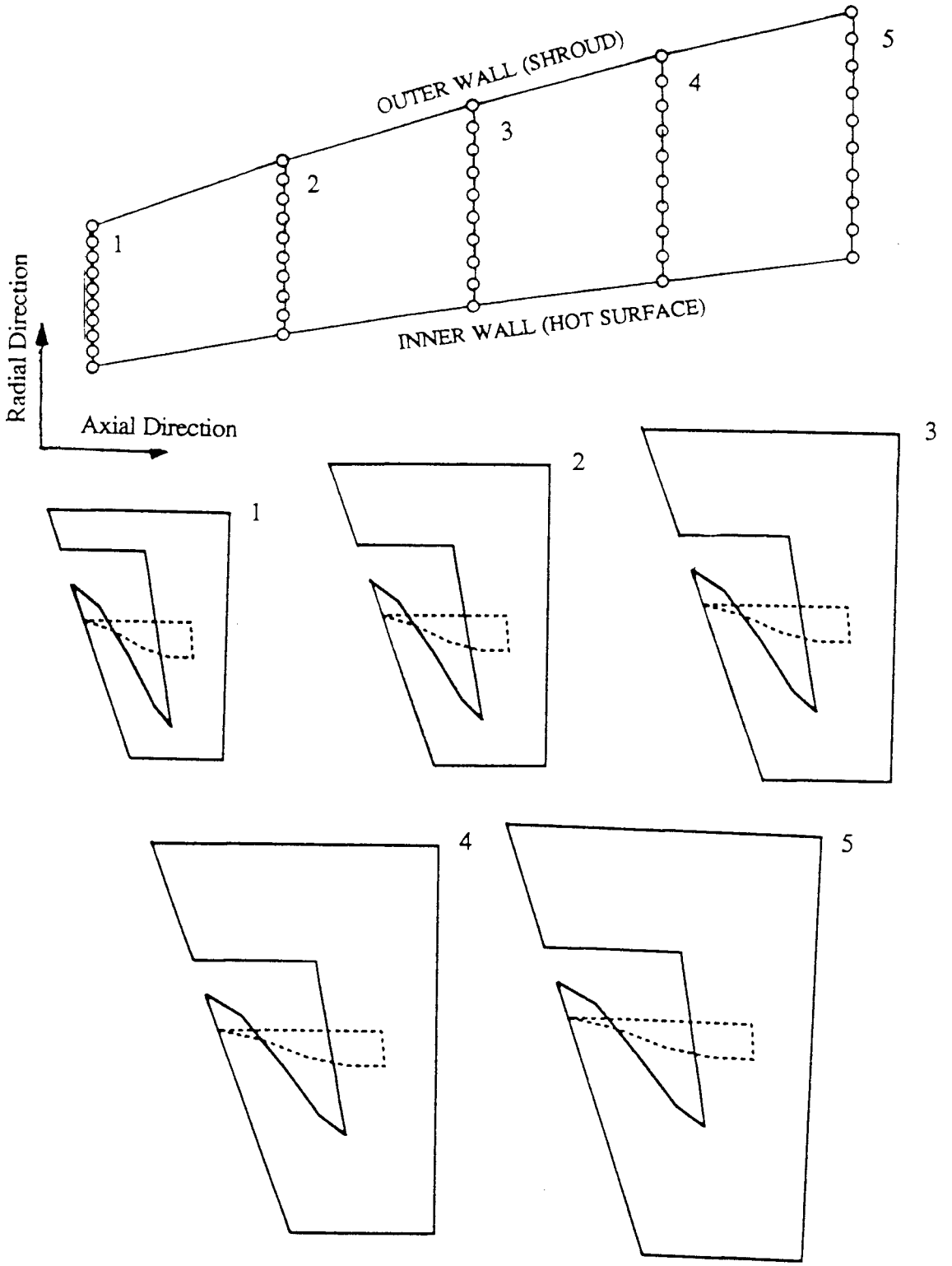

Figure 9. Geometry of a finned coolant flow passage in a parabolic rocket nozzle wall. The top figure shows the outer (shroud) and inner (hot) surfaces and nodes. The five figures below are cross sections at five axial locations showing the initial configuration of the coolant passages (dashed lines) and the fully converged target configurations and the outer wall cross sections (solid lines).